THE JOURNAL OF PHYSICAL CHEMISTRY B

Article

pubs.acs.org/JPCB

Proton Transport in a Membrane Protein Channel: Two-Dimensional Infrared Spectrum Modeling

Chungwen Liang, Jasper Knoester,* and Thomas L. C. Jansen*

Center for Theoretical Physics and Zernike Institute for Advanced Materials, University of Groningen, Nijenborgh 4, 9747 AG Groningen, The Netherlands

ABSTRACT: We model the two-dimensional infrared (2DIR) spectrum of a proton channel to investigate its applicability as a spectroscopy tool to study the proton transport process in biological systems. Proton transport processes in proton channels are involved in numerous fundamental biochemical reactions. However, probing the proton transport process at the molecular level is challenging, because of the limitation in both spatial and time resolution of the traditional experimental approaches. In this paper, we perform proton transport molecular dynamics simulations and model the amide I region of the 2DIR spectrum of a proton channel to examine its sensitivity to the proton transport process. We first report the position dependent proton transfer rates along the channel. The rates in the middle of the channel are larger than those in the entrance. In the presence of protons, we find that the antidiagonal line width of the 2DIR spectrum is larger, and the time evolution of the 2DIR spectrum is slower than that without proton. The time evolution of the 2DIR spectrum with different isotope-labeled residues is similar, even if the local proton transfer rates are different. This results from the proton hopping and the channel water rotation being collective mechanisms, and these effects are convoluted in the spectra.

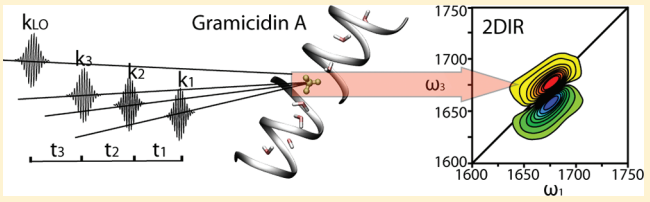

INTRODUCTION

Proton transport in protein channels is essential in a wide variety of biological processes, such as photosynthesis,[1,2] enzyme catalysis,[3,4] bactericidal activity,[5,6] and viral replication.[7,8] Proton channels, which connect the extracellular and cytoplasmic domains of a cell, are mainly embedded in the lipid bilayer, in order to transport protons across the cell membrane. Some proton conduction pathways are formed by the water molecules present inside the protein hydrophilic cavity, which usually changes the water hydrogen bond network from the bulk condition (three-dimensional) to a water-wire-like structure (one-dimensional). Under this confined condition, a proton transfers rapidly and efficiently from a hydronium ion to neighboring water molecules. This is the fundamental concept for the large proton conduction through proton channels.[9] Directly probing proton transport and determining the proton transfer (PT) rates inside narrow channels are the crucial steps for understanding numerous biological processes.

Recent studies[10−17] have demonstrated the potential of two-dimensional infrared spectroscopy (2DIR) to probe molecular scale processes, such as structural dynamics and energy transfer, in a complex molecular environment at time scales down to pico- and femtoseconds. The optically strongly active amide I vibration (C═O stretch), which occurs in peptides and proteins, is the most popular excitation used in 2DIR. The 2DIR experiment is sensitive to the magnitude and time scale of the electric field fluctuations in the environment of amide I oscillators, because these fluctuations affect the vibrational frequency. For the problem of proton transport, the assumption is that the charge of the moving proton (along with other dynamics in the channel) is reflected in fluctuations of the amide I vibrational frequency of proton channels.[18,19] By isotope labeling specific amide I groups, this information can be made site specific, because it allows for spectral separation of this particular site from contributions caused by other amide I vibrations in the channel.[20−24] Due to the heavier mass of the isotope label, its vibrational frequency is red-shifted and results in isolated peaks in the infrared spectra. In previous studies,[25−27] the site-specific information of membrane proteins, such as solvent exposure and protein−lipid interaction, could be probed by measuring the diagonal line width of the isotope-labeled 2DIR spectrum. Thus, by measuring the 2DIR spectrum with different waiting times of each isotope-labeled site, the local dynamics can be revealed from the time evolution of the 2DIR spectrum. This information can be directly compared to the simulated 2DIR spectra containing only a single site. In general, the shape of the peaks in a 2DIR spectrum is determined by the magnitude and time scale of the frequency fluctuations.[14,28−30] If the vibrational frequencies do not have time to change between the pump and the probe (i.e., during the waiting time), the observed peaks will be extended along the diagonal of the 2DIR spectrum. If the frequency fluctuations are faster than the waiting time, the loss of correlation (between the frequency excited at the time of the pump and the frequency detected by the probe) is observed as broadening along the antidiagonal direction, leading to rounder peak shapes. This paper aims at investigating what determines the amide I line shape in a proton channel, and to what extent

Received: February 29, 2012
Revised: May 14, 2012
Published: May 16, 2012

   dx.doi.org/10.1021/jp3019827 | J. Phys. Chem. B 2012, 116, 6336−6345

the proton transport in proton channels can be probed by 2DIR. A key question is how local the dynamical information in the 2DIR spectrum is.

The gramicidin A (gA) peptide is one of the best-characterized prototypic proton channels, and has been the subject of a large amount of experimental[31−34] and theoretical[35−39] studies. It plays an important role in proton/ion transport through cell membranes. The antibiotic activity of the gA channel is a result of increasing the permeability of inorganic monovalent cations through the bacterial cell membrane, thereby destroying the proton/ion gradient between the cytoplasm and the extracellular domains.[40] The active peptide forms a β-helical dimer with a hydrophilic narrow pore (diameter ∼0.4 nm) in the center, allowing a single-file water chain to penetrate. Therefore, the water rotation and diffusion play crucial roles in proton/ion transport.[36,41−43] It has been suggested that the proton transport process in the channel relates to two main mechanisms: proton hopping and water reorientation.[37,43−45] After a proton translocates from one side of the channel to the other side through the single-file water chain, all the water molecules have changed their orientations. If a new proton should be transported along the same direction again, all the water molecules in the channel must first flip back to accommodate this new proton.

The proton transport in channels has been intensively investigated both experimentally[34,46,47] and theoretically[36,41−43,45−48] to get a better understanding of the overall process. The experimental studies have measured the current of a single channel to determine how the proton conductance is affected by local factors, such as variations in the cross membrane potential[34] and the lipid types,[46] and cross-linking both helices that form the channel to change the length of the channel.[47] The theoretical studies have focused on water diffusion in nanopores with classical molecular dynamics (MD) simulations[38,49,50] and proton hopping processes with *ab initio* MD,[41,42] path-integral,[51] multistate empirical valence bond (MS-EVB) methods[45,48] and Monte Carlo simulations.[43] The classical MD simulations use force fields to describe the potential energy surface on which classical nuclei move which prevent proton transfer in the simulations. The other methods apply different electronic structure approximations to obtain these potential energy surfaces. None of the methods applied so far to this problem account for the quantum nature of the nuclei, which is at this point too challenging to account for.[52] Strikingly, previous simulations[41,53] showed that there is a significant enhancement by an order of magnitude of the PT inside narrow hydrophobic channels compared to the bulk condition. However, there is still a gap between simulations and experiments, because the PT rate, especially its position dependence, is difficult to determine by current experimental methods. To obtain an accurate position dependent PT rate which is needed for averaging over a large ensemble, computationally expensive electronic structure based simulation methods, such as Car−Parrinello molecular dynamics (CPMD),[54] cannot be used.

Experimental 2DIR spectra are hard to interpret. Therefore, simulations are needed to understand and analyze experimental results. The simulation of 2DIR experiments currently relies on MD simulations to obtain structural information, and *ab initio* maps to translate this information into a time-dependent vibrational exciton Hamiltonian.[15,55−59] Solving the time-dependent Schrödinger equation for this Hamiltonian then yields the linear infrared absorption and 2DIR spectra.[15,60−64] For the problem of proton transport, using electronic structure based simulation methods, such as CPMD,[54] is too time-consuming to sample enough configurations for modeling the 2DIR spectrum, which require proper ensemble averaging. In a previous study,[18] we used a kinetic model to describe the proton transport in the gA channel with parameters derived from all-atom simulations. We showed that the time evolution of the 2DIR spectrum is sensitive to the magnitude of the PT rate which was chosen position independent along the channel. In the present paper, we report on the results of a more realistic simulation where the gA channel is treated at an atomistic level by combining MD simulations with the Q-HOP method.[65−67] This approach, which is based on a quantum mechanical parametrization of the PT process, allows all-atom simulations for the hundreds of nanoseconds needed to obtain a reasonable ensemble average for the 2DIR simulations. Then, the position dependent PT rates can be directly calculated from simulation trajectories, and the relationship between the time evolution of the 2DIR spectrum and these PT rates may be investigated.

The remainder of this paper is organized as follows. In the Methods section, we will describe all the MD simulation procedures and parameters, and the method for the 2DIR spectrum modeling. In the Results section, we first describe the results obtained from MD simulations and then focus on analyzing the 2DIR spectra. By comparing these results, we can understand how the proton transport influences the spectral line shape. In the end, it will be discussed how the position dependent PT rates along the channel are correlated with the time evolution of the 2DIR spectrum. Finally, conclusions will be drawn.

METHODS

Molecular Dynamics Simulations. Classical MD simulations are performed using the GROMACS 4.5 package[68] with the OPLS-AA force field[69] for the protein, the modified Berger's force field[70] for the lipids, and the SPC/E model[71] for the water molecules. The gA helical-dimer structure is taken from the NMR structure provided in the PDB file 1JNO.[72] Each monomer contains 17 residues and 16 amide I groups. The N-terminal and C-terminal are capped with formyl (FOR) and ethanolamine (ETA), respectively. The gA channel is embedded inside a bilayer of 64 DMPC lipid molecules by using Kandt's method[73] and solvated with 2053 water molecules, as shown in Figure 1. All the water molecules in the system are potential proton acceptors. Then, we add a hydronium and a chlorine ion into the system, which are outside the gA channel. The hydronium ion force field is taken from Lill and Helms.[67]

During all simulations, the SETTLE algorithm[74] is used to constrain bond lengths and angles of the water molecules, and the LINCS algorithm[75] is used for all other bonds and angles involving hydrogen atoms, allowing an integration time step of 2 fs. Long range electrostatic interactions are calculated by the particle mesh Ewald (PME) method[76] with a grid spacing of 0.12 nm. Short-range repulsive and attractive dispersion interactions are described with the Lennard-Jones potentials, using 0.9 nm for the cutoff length. The temperature of the system is kept constant by the Nosé−Hoover coupling method[77,78] on the protein, lipids, and water molecules (including the hydronium and chlorine ions) separately with an external heat bath at 298 K (coupling time 0.1 ps). Similarly, the pressure is kept constant by the semi-isotropic Parrinello−

dx.doi.org/10.1021/jp3019827 | J. Phys. Chem. B 2012, 116, 6336−6345

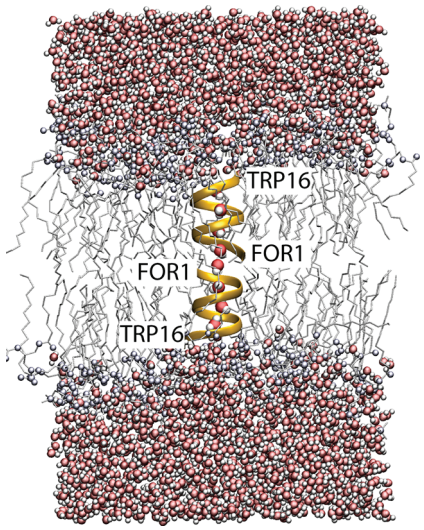

Figure 1. The MD simulation system. The gramicidin A peptides (yellow ribbons) which form a narrow channel with a helical dimer structure are embedded within a DMPC lipid bilayer (headgroup, blue sphere; tail, gray stick) and surrounded by SPC/E water molecules (oxygen, red sphere; hydrogen, white sphere). The amino acid sequence of the gA peptide is FOR1-VAL2-GLY3-ALA4-LEU5-ALA6-VAL7-VAL8-VAL9-TRP10-LEU11-TRP12-LEU13-TRP14-LEU15-TRP16-ETA17.

Rahman coupling[79] method to a pressure bath of 1 bar (coupling time 10 ps).

The Q-HOP method as implemented in GROMACS 3.3[68] is used to simulate proton transport. It is based on quantum mechanically derived proton hopping rates.[65−67] From this semiclassical point of view, the PT process takes place instantaneously between the donor and acceptor, where the hopping probability is parametrized with quantum mechanical methods.[65,66] The transfer probability map is based on two reaction coordinates: the donor−acceptor distance (R_{DA}) and the energy difference between the donor-bound state and the acceptor-bound state (E_{12}). There are three regimes in this probability map. If both R_{DA} and E_{12} are large enough to generate high-energy barriers for PT, transition state theory is used for parametrization. If both R_{DA} and E_{12} are too small to produce energy barriers, the parametrization is based on the numerical solution of the time-dependent Schrödinger equation. Between these two regimes, logarithmic interpolation is used for covering the gap between the two separated regimes mentioned above. We used the parametrization given in refs 65 and 66.

We construct the simulation system in the following steps. After 2 ns of position restrained simulation on all protein atoms, 2 ns position restrained simulation on the protein C_α atoms, and 2 ns simulation without any restrain, the system is assumed to be properly equilibrated. The size of the simulation box is 4.5 × 4.5 × 6.6 nm^3. Then, in order to sample different configurations both of the gA channel and the water molecules inside the channel, trajectory A is generated in production phase for 500 ns with 0.2 ns between each snapshot (2500 frames in total), as illustrated in Figure 2.

For modeling the 2DIR spectrum with proton transport, we start the proton transport simulations beginning with each snapshot from trajectory A. The PT process is treated with the Q-HOP method[67] which has been used for several kinds of systems involving proton transport.[80−83] The Q-HOP method

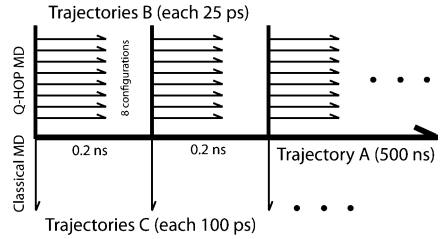

Figure 2. Schematic illustration of the different groups of trajectories. Trajectory A is 500 ns of classical MD simulation. Trajectory B is 500 ns (20 000 × 25 ps) with proton transport simulation. Trajectory C is 250 ns (2500 × 100 ps) with classical MD simulation.

is based on quantum mechanically derived proton hopping rates.[65−67] To simulate a hydronium inside the channel, we swap one of the water molecules inside the channel with the hydronium ion outside the channel. There are at least eight water molecules inside the channel. We swap each of them one by one and then minimize the potential energy of the simulation box to generate eight different starting configurations for proton transport simulation. Before each production run, a 1 ps equilibration run is performed. This results in a total of 20 000 (2500 × 8) proton transport trajectories B, where each is 25 ps long with 20 fs between each snapshot. The total simulation time for proton transport simulation is 500 ns.

For modeling the 2DIR spectrum without proton transport, we also start the classical MD simulations with each snapshot from trajectory A. Leaving the hydronium ion outside the channel, there is no effect of the proton on the amide I groups of the gA channel. We run each configuration for 100 ps with 20 fs between each snapshot. Then, a total of 2500 trajectories C are generated with a total simulation time of 250 ns.

2DIR Spectrum Modeling. The system Hamiltonian of one isotope labeled C═O oscillator is described by the vibrational exciton model:

$$H = \omega(t)B^\dagger B - \frac{\Delta}{2}B^\dagger B^\dagger BB + \vec{\mu}(t)\vec{E}(t)[B^\dagger + B] \quad (1)$$

where $B^\dagger$ and B are Bosonic creation and annihilation operators, respectively, of the isotope labeled oscillator. $\omega(t)$ is the vibrational frequency of the site, Δ = 16 cm^{-1} is the anharmonicity,[23] and $\vec{\mu}$ is the transition dipole responsible for the coupling to the applied laser field $\vec{E}(t)$. The vibrational frequencies are affected by the local environment. The effect of the neighboring units is accounted for with a dihedral map obtained from *ab initio* calculations on glycinedipeptide.[84] The frequency change from the remaining environment is determined with an electrostatic map, which considers the effect of a local electric field and the electric field gradient:[55]

$$\omega_i = \omega_{gas} + \Delta\omega_N(\varphi_{i,i-1}, \psi_{i,i-1}) + \Delta\omega_C(\varphi_{i,i+1}, \psi_{i,i+1}) + \Delta\omega_{map}(E(r), \nabla E(r)) \quad (2)$$

where ω_{gas} is the gas-phase frequency (1717 cm^{-1}). $\Delta\omega_N$ is the frequency shift originating from the previous site $i-1$ toward the N terminus, while $\Delta\omega_C$ is the frequency shift originating from the next site $i+1$ toward the C terminus. $\Delta\omega_{map}$ is the frequency shift due to the electric field generated by surrounding molecules.[55] We used the OPLS-AA force field for calculating the amide-I frequency shift, which are the same charges as those used in the MD simulation. The charges of the

dx.doi.org/10.1021/jp3019827 | J. Phys. Chem. B 2012, 116, 6336−6345

nearest neighbor amide-I units and the charges beyond the cutoff (2 nm) are excluded. Other charges of the peptides, water, and lipids within the cutoff are all included. This and similar approaches have been successfully applied previously.[62,85,86]

After constructing the time dependent Hamiltonian for an oscillator in a fluctuating environment, 2DIR spectra are calculated by using the numerical integration of the Schrödinger equation (NISE) method.[61,87] This approach is based on numerically solving the time-dependent Schrödinger equation for the vibrational Hamiltonian and using the solution to calculate response functions. In this method, the Hamiltonian is considered to be constant for a short time interval (20 fs). During each of these time intervals, the time independent Schrödinger equation can then be solved. The time evolution for longer time is determined by successive propagation during short time intervals. We use an ad hoc vibrational lifetime 1 ps for the single excited state of the amide I vibration. The time domain response functions governing the 2DIR signal are then calculated by averaging over multiple starting configurations. We use 240 000 (125 000) configurations for modeling the 2DIR spectrum with (without) proton transport. The frequency domain spectra are calculated as a double Fourier transform of the time domain response functions.

RESULTS

Molecular Dynamics Simulations. The position dependent PT rate (k_{pt}) is calculated along the channel axis and shown in Figure 3a. The channel axis is defined as the principal axis of the gA peptide backbone atoms, denoted by Z. The channel center ($Z = 0$) is then defined as the center of mass of the gA peptide backbone atoms projected along the channel axis. We obtained the PT rates through $k_{pt} = (1/\langle T \rangle)$, where $\langle T \rangle$ is the average lifetime of the hydronium ion. The lifetime T is defined as the duration that the proton stays on a certain water molecule. Within this time duration, the average position of the hydronium oxygen along the channel is also calculated. We calculated the histogram of the position dependence of the lifetime, and symmetrized it by averaging the left-hand and right-hand sides with regard to the channel center; the error bars were calculated from the difference between the two sides. In the membrane/water interfacial region, the PT rate is ~1.7 ps^{-1}. This is slightly higher than the rate in bulk water where a value of 1.23 ps^{-1} was reported with simulations using the same method as here.[83] For bulk water, the experimental value measured by pump−probe infrared spectroscopy is 1.2 ps^{-1},[88] and a value of 0.67 ps^{-1} was measured by NMR.[89] Further into the channel center, the PT rate increases to its maximum value (~10 ps^{-1}) around the position of ALA4; then, it decreases to a lower value (~8.5 ps^{-1}) at the center. This shows that the proton hopping is at least 5 times faster in the channel center than at the entrance. To understand the location of each residue and lipid head groups, the peak height normalized distributions of the carbonyl carbon positions of the isotope-labeled residues and the position of the lipid nitrogen and phosphorus atoms along the channel axis are shown in Figure 3b.

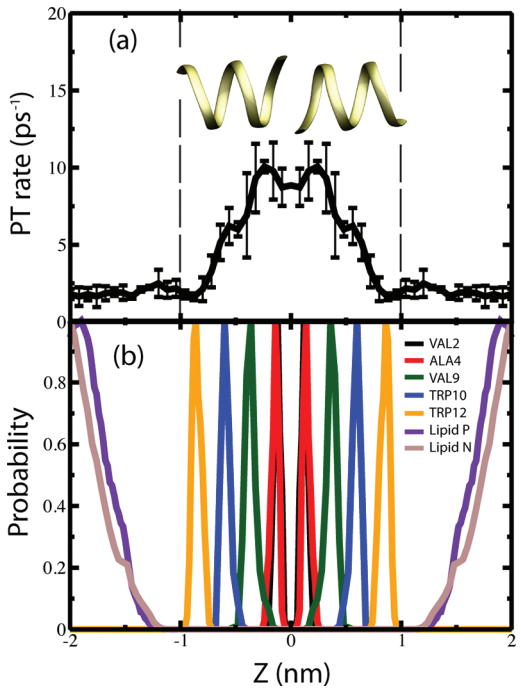

Figure 3. (a) Position dependent PT rate along the gA channel. The gA channel is shown as yellow ribbons. (b) The peak height normalized distributions of the carbonyl carbon positions of isotope-labeled residues and the position of the lipid nitrogen/phosphorus atom along the channel axis.

2DIR Spectrum Modeling. First, we simulated the isotope-labeled 2DIR spectra of each residue in the gA helical dimer from trajectories without a proton in the channel (shown in Figure 4). All the calculated 2DIR spectra correspond to the experimental setup, where all the laser pulses are polarized in the same direction (the parallel polarization setup). The spectra are symmetrized by averaging over the two symmetry related sites of the gA dimer. This allows us to understand the site dependence of the local dynamics along the gA channel. In general, the isotope-labeled residues with a single peak in the spectrum are close to the channel center; however, there are some residues showing two peaks along the diagonal, such as ALA6, VAL9, TRP10, etc. Diagonal slices of the isotope-labeled 2DIR spectra are shown in Figure 5. To elucidate the origin of the two peaks structure appearing in some residues, we calculated the correlation between the frequency and the distance between the carbonyl oxygen and the closest water hydrogen. The result is shown in Figure 6a. This shows that there is a positive correlation between them: the less the distance, the lower the frequency. The two dominant configurations involved in the interaction between an amide I group and water molecules are illustrated in Figure 6b. If a channel water molecule forms a hydrogen bond to the carbonyl oxygen on the isotope-labeled residue, the frequency will be red-shifted. If there is no hydrogen bonding between the carbonyl oxygen and channel water molecules, the frequency will be higher. In ALA6 and TRP10, both structures are present, which results in two peaks along the diagonal in the 2DIR spectrum. However, in ALA4 and TRP12, the non-hydrogen-bonded and the hydrogen-bonded structures dominate, respectively. This results in either a single low or high frequency peak along the diagonal in the isotope-labeled 2DIR spectrum.

To understand how the proton transport changes the dynamics of the local environment, we calculated the diagonal line width as a function of residue number shown in Figure 7a based on trajectories B and C. The diagonal line width is taken

dx.doi.org/10.1021/jp3019827 | J. Phys. Chem. B 2012, 116, 6336−6345

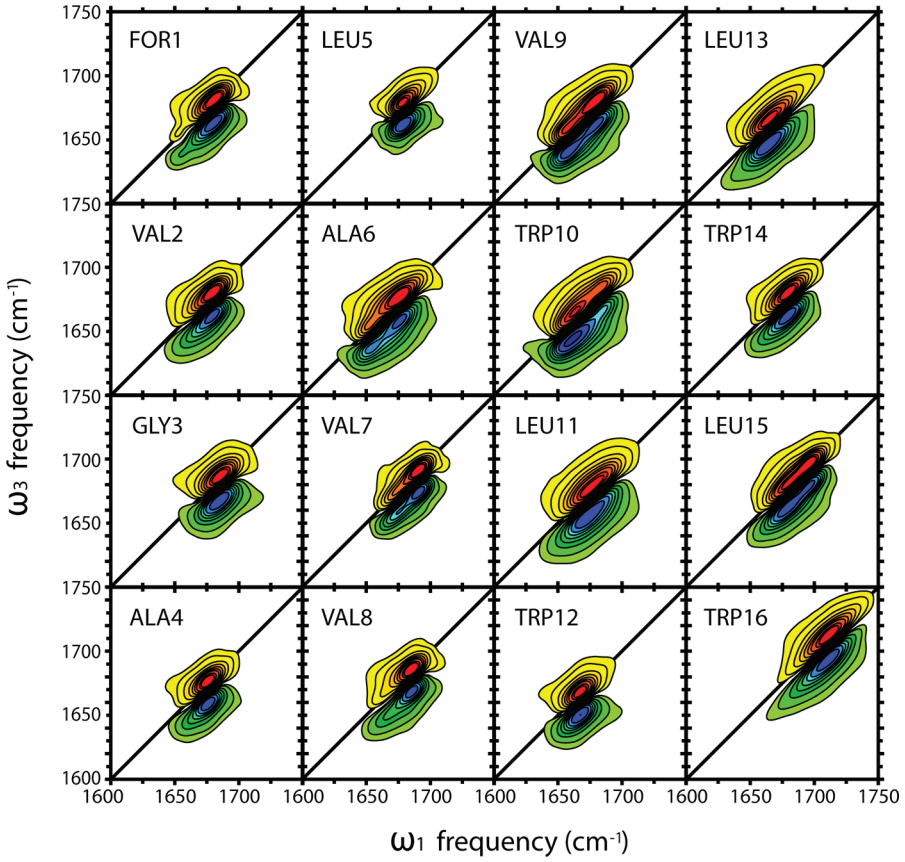

Figure 4. 2DIR spectra of isolated isotope-labeled units (without proton) for all residues using zero waiting time. Each color contour represents 10% of the maximal amplitude.

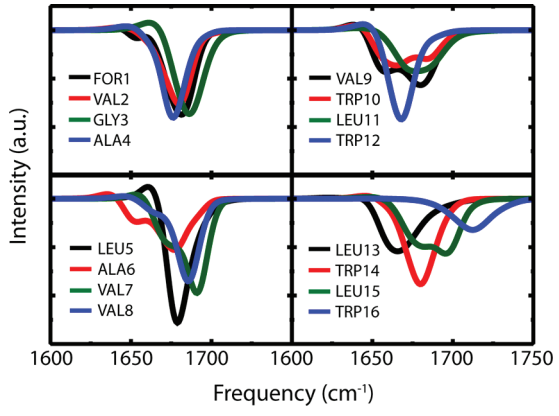

Figure 5. Diagonal slices of the 2DIR spectra in Figure 4.

as the full width at half-maximum (fwhm) of the slice along the diagonal. In general, the diagonal line width of the isotope-labeled residue close to the channel center is smaller than that of the residue nearby the channel entrance. This shows that the polar lipid head groups and the interfacial water molecules generate larger electric field fluctuations than the nonpolar lipid tails around the central region of the gA channel.[18] When proton transport takes place, the diagonal line width becomes a few wavenumbers higher in the channel center (from residue VAL2 to LEU5), and with larger difference on the residue ALA6 and VAL7, but there is no significant effect on the channel entrance (from residue VAL9 to TRP16). We calculate the antidiagonal line width shown in Figure 7b. This line width is taken as the fwhm of the slice which intersects perpendicularly to the diagonal at the frequency where the linear absorption peaks. We found that the proton induces a larger line width for all residues. For LEU5 and VAL8, the diagonal line width seems to change a lot when a proton is added. This is an artifact arising from the fact that the peaks contain a substructure of at least two peaks. The relative peak intensity changes very slightly when adding the proton, resulting in the contribution from the lower one of the two peaks just crossing the half intensity line. Thus, when there is no proton, the lower one of the two peaks does not contribute to the diagonal line width. However, when the proton is present, it has a significant contribution, but the overall change in line shape is very limited. This artifact is not significant for the antidiagonal line width, as there are no significant side peaks in that direction.

To investigate the time evolution of the system, we modeled the isotope-labeled 2DIR spectra of three residues (VAL2, ALA4, and TRP12) with 10 different waiting times t_2 between 0 and 5 ps, because the single peak structures are easier to analyze quantitatively. We limited our simulations to 5 ps, because in practice the ~1 ps vibrational lifetime precludes accurate measurements of the 2DIR spectrum at longer times. The 2DIR spectra of the investigated residues are shown in Figure 8 for three different waiting times. Then, we calculated the antidiagonal line width, diagonal line width, and the intensity-weighted slope of the isotope-labeled 2DIR spectrum for each residue as a function of waiting time t_2. These are all shown in Figure 9. The intensity-weighted slope is defined as

dx.doi.org/10.1021/jp3019827 | J. Phys. Chem. B 2012, 116, 6336−6345

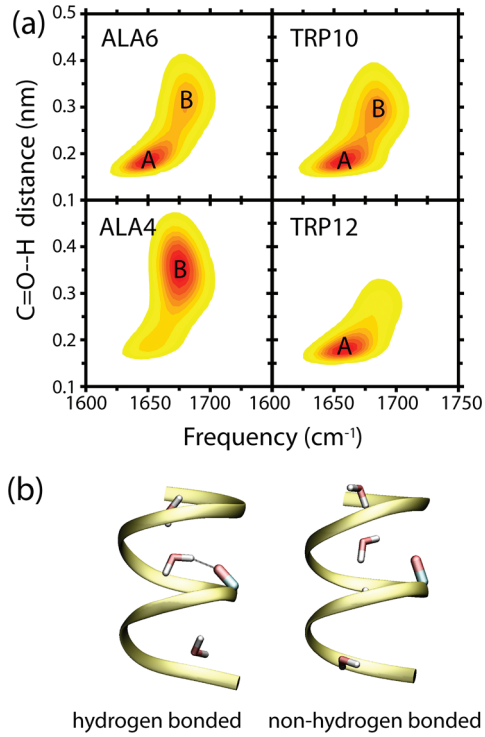

Figure 6. (a) The two-dimensional correlation plot between the site frequency and the minimal distance between the carbonyl oxygen and water hydrogens of ALA4, ALA6, TRP10, and TRP12. (b) The two structures with and without hydrogen bonding to a water molecule illustrated for ALA6.

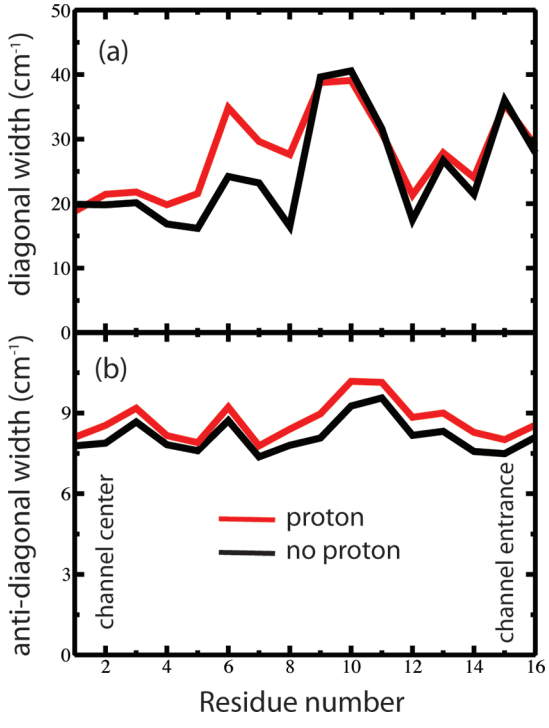

Figure 7. Lineshape parameters extracted from simulated 2DIR spectra of isotope-labeled residues: (a) diagonal line width and (b) antidiagonal line width as functions of residue number.

$$\langle S \rangle = \frac{\int I_{max}(\omega_1) S_{max}(\omega_1)\, d\omega_1}{\int I_{max}(\omega_1)\, d\omega_1} \quad (3)$$

First, we determined the maximum intensity of the diagonal peak along ω_3 for each ω_1; then, we connected the thus generated collection of points for different ω_1 to define the max line. $I_{max}(\omega_1)$ is the intensity along the max line, and $S_{max}(\omega_1)$ is the slope of the max line. $\langle S \rangle$ is, thus, the weighted average slope value of the peak. The plots in Figure 9 were fitted to an exponential function with an offset. The fit parameters are shown in Table 1. The decay times τ reveal the effect of the proton transport. It is observed that, when there is no proton inside the channel, the three residues (VAL2, ALA4, and TRP12) have different offsets in the antidiagonal line width and slope. When proton transport takes place, the antidiagonal line width and slope of these three residues behave similarly, and the decay times τ of these quantities (in Table 1) increase to about twice the decay times τ without proton transport. This is evidence that proton transport changes the system dynamics, and this can be directly probed by 2DIR.

To illustrate how the proton affects the amide I frequency, we calculated the distribution of the site frequencies as a function of hydronium oxygen position along the channel axis (see Figure 10). We first calculated the correlation between site frequency and the hydronium oxygen position. The max lines calculated as above are shown as thick solid lines. The width of the frequency distribution of each slice along the channel axis is shown with the dashed lines. These were obtained as the fwhm of each vertical slice. It can be seen that the site frequencies depend on the hydronium position and the amide I group orientation. When a proton approaches an amide I group with a dipole moment pointing along the negative Z direction (ALA4 and VAL8) from the right side, the site frequency decreases due to the proton electrostatic effect. When the proton passes the amide I group, the site frequency first increases and then it decreases again when the proton is further away from the amide I group. VAL2 behaves similar to ALA4 (data not shown), due to the fact that their positions along the channel are very close. For the amide I groups with the reverse orientation (LEU5), the site frequency behaves in the opposite way. For the amide I groups close to the channel entrance (TRP12), the proton effect is less pronounced due to the effect from the lipid head groups. This shows that a proton generates a long-range effect on the site frequencies over a length of at least 1 nm, which is the half size of the gA channel, thereby inhibiting the possibility to obtain detailed local information.

DISCUSSION

Proton transport in membrane proteins has been intensively studied by different simulation approaches, including MS-EVB,[45,90,91] CPMD,[92,93] path-integral,[51] semiclassical,[37] and Monte Carlo[43] methods, in order to derive the free energy surface for proton translocation along these channels. However, due to the limited simulation time (from ps to tens of ns), the PT rate along the channel is difficult to determine. We determined the position dependent PT rates along the gA channel from our Q-HOP trajectories. The rates in the channel center are ~10 ps^{-1}, which is at least 5 times higher than that close to the channel entrance. This can be explained by the formation of a water-wire-like structure[41,53] inside channel, and recent research has found that PT is highly efficient along such wires.[41,53,83,93,94] In a narrow channel, the water molecules near the center are more ordered than the water molecules which interact with lipid head groups or interfacial water at the entrance. The electrostatic potential across the lipid bilayer also contributes to the fast PT in the channel center.[90] The PT rates

dx.doi.org/10.1021/jp3019827 | J. Phys. Chem. B 2012, 116, 6336−6345

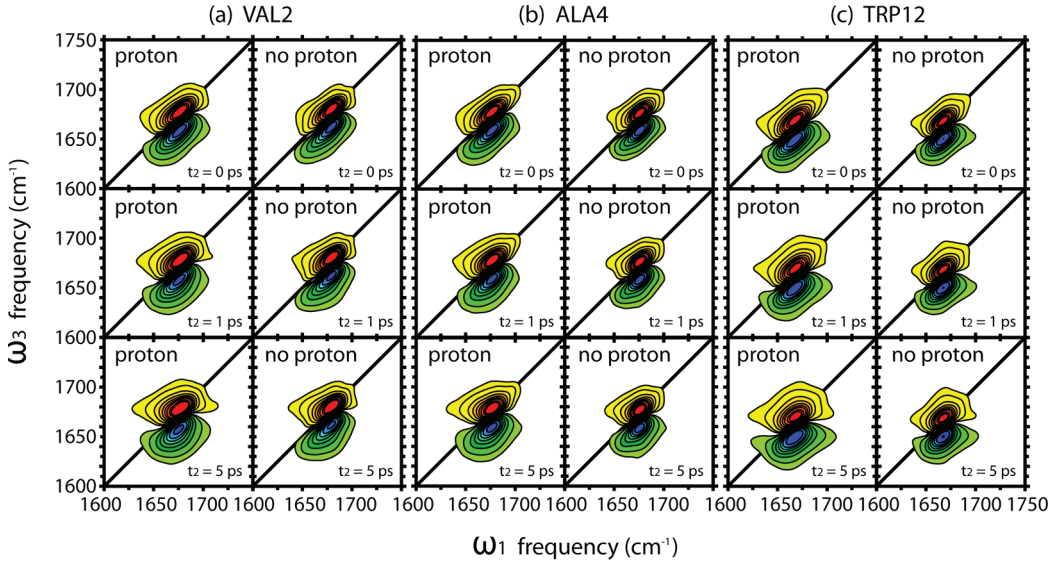

Figure 8. 2DIR spectra of isolated isotope-labeled units (a) VAL2, (b) ALA4, and (c) TRP12 with waiting times t_2 of 0, 1, and 5 ps. The 2DIR spectra with a proton are shown in the left side columns of parts a, b, and c. The 2DIR spectra without a proton are shown in the right side columns. Each color contour represents 10% of the maximal amplitude.

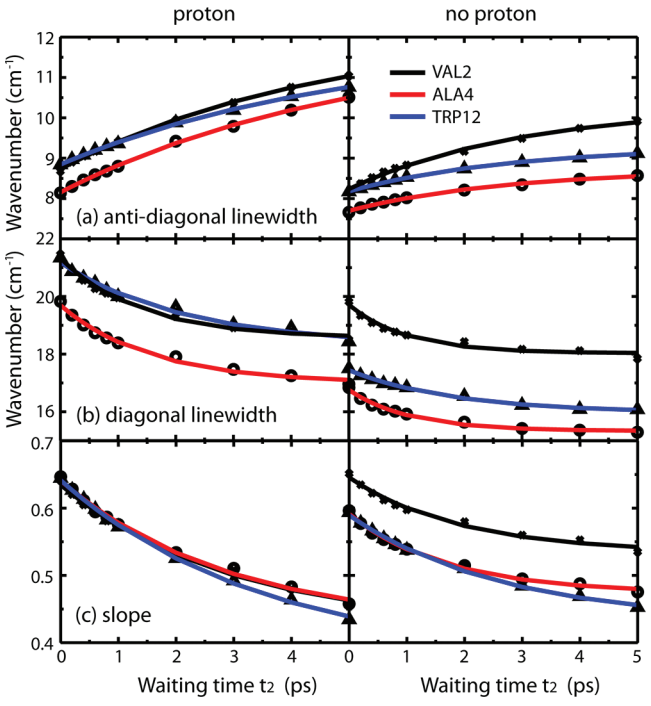

Figure 9. Time evolution of line shape parameters extracted from the isotope-labeled 2DIR spectra: (a) antidiagonal line width, (b) diagonal line width, and (c) intensity-weighted slope value as functions of waiting time.

Table 1. Fitting Parameters of Anti-Diagonal Linewidth (Anti), Diagonal Linewidth (Diag), and the Intensity-Weighted Slope (Slope) as a Function of the Waiting Time as Shown in Figure 9[a]

proton				no proton			
anti	A_1	τ	A_2	anti	A_1	τ	A_2
VAL2	3.5	4.6	8.7	VAL2	2.0	3.0	8.2
ALA4	3.7	5.1	8.2	ALA4	1.0	2.7	7.7
TRP12	3.0	5.0	8.8	TRP12	1.1	2.8	8.2
diag	A_1	τ	A_2	diag	A_1	τ	A_2
VAL2	2.8	1.4	19	VAL2	1.7	1.0	18
ALA4	2.7	1.6	17	ALA4	1.4	1.1	15
TRP12	2.9	2.2	18	TRP12	1.5	1.8	16
slope	A_1	τ	A_2	slope	A_1	τ	A_2
VAL2	0.21	2.9	0.42	VAL2	0.11	1.9	0.53
ALA4	0.22	2.9	0.43	ALA4	0.12	1.7	0.47
TRP12	0.27	3.5	0.38	TRP12	0.16	2.7	0.43

[a]The exponential functions with offset are chosen as $A_1 \times \exp(-t/\tau) + A_2$ for diagonal linewidth and slope and $A_1 \times (1 - \exp(-t/\tau)) + A_2$ for the anti-diagonal linewidth.

on the inverse pico-second time scale show that the proton hopping mechanism should not be the limiting step for proton transport through membrane protein channels. In our simulation, we found that protons have a low probability to enter the channel from the bulk region, but they escape easily from the channel to the bulk. Therefore, the process of a proton entering the channel appears to be the key limiting step. This means that only at low pH one can expect a proton to be present inside the channel a significant amount of time. Therefore, to probe proton transport in membrane proteins, we expect that the 2DIR experiment will only be sensitive at low pH. The entering of the proton into the channel in itself would be an interesting topic of future research, as this appears to be an important bottleneck.

The time evolution of the isotope-labeled 2DIR spectra of different residues is similar, even though the local PT rates are different. This is attributed to the proton long-range electrostatic effect and the collective motion of the proton hopping and the water rotation.[18] We observed that, even when a proton moves around the channel entrance, the frequency fluctuation of the amide I vibration at sites in the channel center still correlates with the dynamics of the proton at the channel entrance. We found that the correlation distance is in the order of 1 nm, indeed extending over most of the channel. The 2DIR spectra of different units exhibit similar behavior in the presence of a proton, and the experiment is expected to be

dx.doi.org/10.1021/jp3019827 | J. Phys. Chem. B 2012, 116, 6336−6345

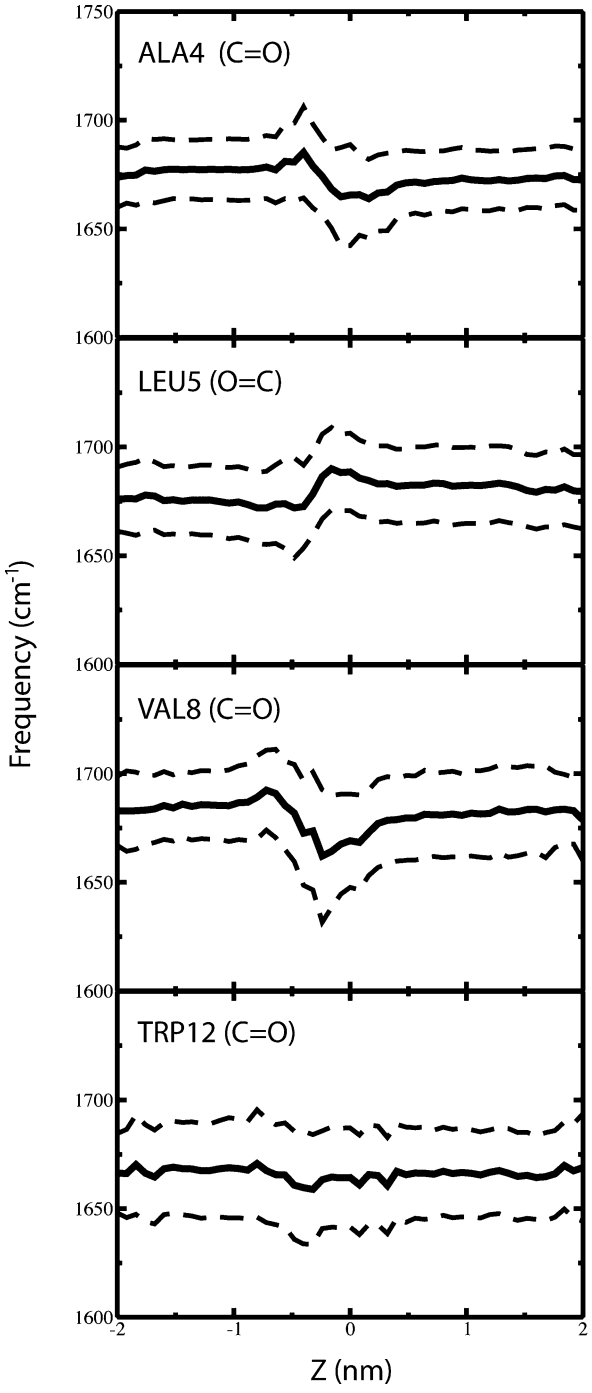

Figure 10. The site frequencies as a function of the hydronium ion position along the channel axis. The dashed lines show where the probability is half of the probability at the max line, thus indicating the fwhm of the frequency distribution at a given hydronium position.

sensitive only to the average proton hopping rate inside the channel, and not to its local variations.

It is known that the Q-HOP method violates the detailed balance,[67] which results in the unreliable calculations of statistical mechanics properties, such as the PT rates in this paper. However, the essential observation of this paper, that the PT rates are larger in the channel center than in the channel entrance, is in good agreement with previous studies.[41,53] To this end, one would expect that our results should be validated by experimental observations and theoretical improvements in the future.

CONCLUSIONS

In this paper, we performed MD simulations and 2DIR spectrum modeling to study proton transport through the gA channel. The position dependent PT rates were calculated on the basis of extensive proton transport simulations. The PT rates in the channel center are at least 5 times higher than those close to the channel entrance. We also found that the proton transport indeed changes the system dynamics which can be revealed by measuring the time evolution of the antidiagonal line width and slope of the 2DIR spectrum. The position dependent PT rates are smeared out in the measured isotope-labeled 2DIR spectrum, due to the collective mechanisms involving proton hopping and channel water rotation. The local amide I site frequencies are sensitive to proton hopping within a range of about 1 nm.

Besides proton channels, some other systems involving proton transport, such as enzyme families,[91] condensed phase crystals,[95,96] carbon nanotubes,[94] and fuel cell electrolyte membranes,[82,97] are also under investigation to understand the proton transport process and determine rate limiting steps. Combining MD simulation and 2DIR spectrum modeling offers a promising tool to study proton transport in these novel systems.

AUTHOR INFORMATION

Corresponding Author

*E-mail: J.Knoester@rug.nl (J.K.); T.L.C.Jansen@rug.nl (T.L.C.J.).

Notes

The authors declare no competing financial interest.

ACKNOWLEDGMENTS

T.L.C.J. acknowledges The Netherlands Organization for Scientific Research (NWO) for support through a VIDI grant. We thank Dr. G. Groenhof, Prof. S. Garrett-Roe, and Prof. M. Zanni for useful discussions.

REFERENCES

(1) Liu, Z.; Yan, H.; Wang, K.; Kuang, T.; Zhang, J.; Gui, L.; An, X.; Chang, W. *Nature* **2004**, *428*, 287−292.
(2) Murakami, M.; Kouyama, T. *Nature* **2008**, *453*, 363−367.
(3) Benkovic, S. J.; Hammes-Schiffer, S. *Science* **2003**, *301*, 1196−1202.
(4) Sytina, O. A.; Heyes, D. J.; Hunter, C. N.; Alexandre, M. T.; van Stokkum, I. H. M.; van Grondelle, R.; Groot, M. L. *Nature* **2008**, *456*, 1001−1004.
(5) Urry, D. W. *Proc. Natl. Acad. Sci. U.S.A.* **1971**, *68*, 672−676.
(6) Burkhart, B. M.; Gassman, R. M.; Langs, D. A.; Pangborn, W. A.; Duax, W. L.; Pletnev, V. *Biopolymers* **1999**, *51*, 129−144.
(7) Schnell, J. R.; Chou, J. J. *Nature* **2008**, *451*, 591−595.
(8) Sharma, M.; Yi, M.; Dong, H.; Qin, H.; Peterson, E.; Busath, D. D.; Zhou, H.; Cross, T. A. *Science* **2010**, *330*, 509−512.
(9) Wraight, C. A. *Biochim. Biophys. Acta* **2006**, *1757*, 886−912.
(10) Hamm, P.; Lim, M.; DeGrado, W. F.; Hochstrasser, R. M. *Proc. Natl. Acad. Sci. U.S.A.* **1999**, *96*, 2036−2041.
(11) Asbury, J. B.; Steinel, T.; Kwak, K.; Corcelli, S. A.; Lawrence, C. P.; Skinner, J. L.; Fayer, M. D. *J. Chem. Phys.* **2004**, *121*, 12431−12446.
(12) Jansen, T. L. C.; Knoester, J. *Acc. Chem. Res.* **2009**, *42*, 1405−1411.
(13) Lin, Y. S.; Shorb, J. M.; Mukherjee, P.; Zanni, M. T.; Skinner, J. L. *J. Phys. Chem. B* **2009**, *113*, 592−602.

(14) Cho, M. *Chem. Rev.* **2008**, *108*, 1331−1418.
(15) Zhuang, W.; Hayashi, T.; Mukamel, S. *Angew. Chem., Int. Ed.* **2009**, *48*, 3750−3781.
(16) Park, S.; Odelius, M.; Gaffney, K. J. *J. Phys. Chem. B* **2009**, *113*, 7825−7835.
(17) Bagchi, S.; Charnley, A. K.; Smith, A. B.; Hochstrasser, R. M. *J. Phys. Chem. B* **2009**, *113*, 8412−8417.
(18) Liang, C.; Jansen, T. L. C.; Knoester, J. *J. Chem. Phys.* **2011**, *134*, 044502.
(19) Ghosh, A.; Qiu, J.; DeGrado, W. F.; Hochstrasser, R. M. *Proc. Natl. Acad. Sci. U.S.A.* **2011**, *108*, 6115−6120.
(20) Woutersen, S.; Hamm, P. *J. Chem. Phys.* **2001**, *115*, 7737−7744.
(21) Demirdöven, N.; Cheatum, C. M.; Chung, H. S.; Khalil, M.; Knoester, J.; Tokmakoff, A. *J. Am. Chem. Soc.* **2004**, *126*, 7981−7990.
(22) Smith, A. W.; Chung, H. S.; Ganim, Z.; Tokmakoff, A. *J. Phys. Chem. B* **2005**, *109*, 17025−17027.
(23) Hamm, P.; Lim, M. H.; Hochstrasser, R. M. *J. Phys. Chem. B* **1998**, *102*, 6123.
(24) Mukherjee, P.; Krummel, A. T.; Fulmer, E. C.; Kass, I.; Arkin, I. T.; Zanni, M. T. *J. Chem. Phys.* **2004**, *120*, 10215.
(25) Fang, C.; Senes, A.; Cristian, L.; DeGrado, W. F.; Hochstrasser, R. M. *Proc. Natl. Acad. Sci. U.S.A.* **2006**, *103*, 16740−16745.
(26) Manor, J.; Mukherjee, P.; Lin, Y. S.; Leonov, H.; Skinner, J. L.; Zanni, M. T.; Arkin, I. T. *Structure* **2009**, *17*, 247−254.
(27) Woys, A. M.; Lin, Y. S.; Reddy, A. S.; Xiong, W.; de Pablo, J. J.; Skinner, J. L.; Zanni, M. T. *J. Am. Chem. Soc.* **2010**, *132*, 2832−2838.
(28) Hybl, J. D.; Christophe, Y.; Jonas, D. M. *Chem. Phys.* **2001**, *266*, 295.
(29) Roberts, S. T.; Loparo, J. J.; Tokmakoff, A. *J. Chem. Phys.* **2006**, *125*, 084502.
(30) Kwak, K.; Rosenfeld, D. E.; Fayer, M. D. *J. Chem. Phys.* **2008**, *128*, 204505.
(31) Andersen, O. S. *Annu. Rev. Physiol.* **1984**, *46*, 531−548.
(32) Wallace, B. A. *Annu. Rev. Biophys. Chem.* **1990**, *19*, 127−157.
(33) Koeppe, R. E.; Andersen, O. S. *Annu. Rev. Biophys. Biomech.* **1996**, *25*, 231−258.
(34) Chernyshev, A.; Cukierman, S. *Biophys. J.* **2002**, *82*, 182−192.
(35) Roux, B.; Karplus, M. *Annu. Rev. Biophys. Biomol. Struct.* **1994**, *23*, 731−761.
(36) Woolf, T. B.; Roux, B. *Proteins: Struct., Funct., Genet.* **1996**, *24*, 92−114.
(37) Pomés, R.; Roux, B. *Biophys. J.* **2002**, *82*, 2304−2316.
(38) de Groot, B. L.; Tieleman, D. P.; Pohl, P.; Grubmuller, H. *Biophys. J.* **2002**, *82*, 2934−2942.
(39) Bastug, T.; Gray-Weale, A.; Patra, S. M.; Kuyucak, S. *Biophys. J.* **2006**, *90*, 2285−2296.
(40) Bourinbaiar, A. S.; Coleman, C. F. *Arch. Virol.* **1997**, *142*, 2225−2235.
(41) Dellago, C.; Naor, M. M.; Hummer, G. *Phys. Rev. Lett.* **2003**, *90*, 105902.
(42) Mann, D. J.; Halls, M. D. *Phys. Rev. Lett.* **2003**, *90*, 195503.
(43) Till, M. S.; Essigke, T.; Becker, T.; Ullmann, G. M. *J. Phys. Chem. B* **2008**, *112*, 13401−13410.
(44) Agmon, N. *J. Chem. Phys.* **1996**, *93*, 1714−1736.
(45) Braun-Sand, S.; Burykin, A.; Chu, Z. T.; Warshel, A. *J. Phys. Chem. B* **2005**, *109*, 583−592.
(46) Chernyshev, A.; Cukierman, S. *Biophys. J.* **2006**, *91*, 580−587.
(47) Narayan, S.; Wyatt, D. L.; Crumrine, D. S.; Cukierman, S. *Biophys. J.* **2007**, *93*, 1571−1579.
(48) Voth, G. A. *Acc. Chem. Res.* **2006**, *39*, 143−150.
(49) Portella, G.; Pohl, P.; de Groot, B. L. *Biophys. J.* **2007**, *92*, 3930−3937.
(50) Portella, G.; de Groot, B. L. *Biophys. J.* **2009**, *96*, 925−938.
(51) Pomés, R.; Roux, B. *Biophys. J.* **1996**, *71*, 19−39.
(52) Markland, T. E.; Habershon, S.; Manolopoulos, D. E. *J. Chem. Phys.* **2008**, *128*, 194506.
(53) Brewer, M. L.; Schmitt, U. W.; Voth, G. A. *Biophys. J.* **2001**, *80*, 1691−1702.
(54) Car, R.; Parrinello, M. *Phys. Rev. Lett.* **1985**, *55*, 2471−2474.
(55) Jansen, T. L. C.; Knoester, J. *J. Chem. Phys.* **2006**, *124*, 044502.
(56) Wang, L.; Middleton, C. T.; Zanni, M. T.; Skinner, J. L. *J. Phys. Chem. B* **2011**, *115*, 3713.
(57) Torii, H.; Tasumi, M. *J. Raman Spectrosc.* **1998**, *29*, 81.
(58) Ham, S.; Kim, J. H.; Lee, H.; Cho, M. H. *J. Chem. Phys.* **2003**, *118*, 3491.
(59) Gorbunov, R. D.; Kosov, D. S.; Stock, G. *J. Chem. Phys.* **2005**, *122*, 224904.
(60) Torii, H. *J. Phys. Chem. A* **2006**, *110*, 9469−9477.
(61) Jansen, T. L. C.; Knoester, J. *J. Phys. Chem. B* **2006**, *110*, 22910−22916.
(62) Auer, B. M.; Skinner, J. L. *J. Phys. Chem. B* **2009**, *113*, 4125−4130.
(63) Paarmann, A.; Hayashi, T.; Mukamel, S.; Miller, R. J. D. *J. Chem. Phys.* **2009**, *130*, 204110.
(64) Falvo, C.; Palmieri, B.; Mukamel, S. *J. Chem. Phys.* **2009**, *130*, 184501.
(65) Lill, M. A.; Helms, V. *J. Chem. Phys.* **2001**, *114*, 1125−1132.
(66) Lill, M. A.; Helms, V. *J. Chem. Phys.* **2001**, *115*, 7985−7992.
(67) Lill, M. A.; Helms, V. *J. Chem. Phys.* **2001**, *115*, 7993−8005.
(68) Lindahl, E.; Hess, B.; van der Spoel, D. *J. Mol. Model.* **2001**, *7*, 306−317.
(69) Jorgensen, W. L.; Tirado-Rives, J. *J. Am. Chem. Soc.* **1988**, *110*, 1657−1666.
(70) Tieleman, D. P.; MacCallum, J. L.; Ash, W. L.; Kandt, C.; Xu, Z.; Monticelli, L. *J. Phys.: Condens. Matter* **2006**, *18*, S1221−S1234.
(71) Berendsen, H. J. C.; Grigera, J. R.; Straatsma, T. P. *J. Phys. Chem.* **1987**, *91*, 6269−6271.
(72) Townsley, L. E.; Tucker, W. A.; Sham, S.; Hinton, J. F. *Biochemistry* **2001**, *40*, 11676−11686.
(73) Kandt, C.; Ash, W. L.; Tieleman, D. P. *Methods* **2007**, *41*, 475−488.
(74) Miyamoto, S.; Kollman, P. A. *J. Comput. Chem.* **1992**, *13*, 952−962.
(75) Hess, B.; Bekker, H.; Berendsen, H. J. C.; Fraaije, J. G. E. M. *J. Comput. Chem.* **1998**, *18*, 1463−1472.
(76) Darden, T.; York, D.; Pedersen, L. *J. Chem. Phys.* **1993**, *98*, 10089−10092.
(77) Nosé, S. *Mol. Phys.* **1984**, *52*, 255−268.
(78) Hoover, W. G. *Phys. Rev. A* **1985**, *31*, 1695−1697.
(79) Parrinello, M.; Rahman, A. *J. Appl. Phys.* **1981**, *52*, 7182−7190.
(80) Lill, M. A.; Helms, V. *Proc. Natl. Acad. Sci. U.S.A.* **2002**, *99*, 2778−2781.
(81) de Groot, B. L.; Frigato, T.; Helms, V.; Grubmüller, H. *J. Mol. Biol.* **2003**, *333*, 279−293.
(82) Devanathan, R.; Venkatnathan, A.; Rousseau, R.; Dupuis, M.; Frigato, T.; Gu, W.; Helms, V. *J. Phys. Chem. B* **2010**, *114*, 13681−13690.
(83) Liang, C.; Jansen, T. L. C. *J. Chem. Phys.* **2011**, *135*, 114502.
(84) Jansen, T. L. C.; Dijkstra, A. G.; Watson, T. M.; Hirst, J. D.; Knoester, J. *J. Chem. Phys.* **2006**, *125*, 44312.
(85) Jansen, T. L. C.; Knoester, J. *Biophys. J.* **2008**, *94*, 1818−1825.
(86) Sengupta, N.; Maekawa, H.; Zhuang, W.; Toniolo, C.; Mukamel, S.; Tobias, D. J.; Ge, N. H. *J. Phys. Chem. B* **2009**, *113*, 12037−12049.
(87) Jansen, T. L. C.; Auer, B. M.; Yang, M.; Skinner, J. L. *J. Chem. Phys.* **2010**, *132*, 224503.
(88) Bakker, H. J.; Rezus, Y. L. A.; Timmer, R. L. A. *J. Phys. Chem. A* **2008**, *112*, 11523.
(89) Luz, Z.; Meiboom, S. *J. Am. Chem. Soc.* **1964**, *86*, 4768−4769.
(90) Qin, Z.; Tepper, H. L.; Voth, G. A. *J. Phys. Chem. B* **2007**, *111*, 9931−9939.
(91) Maupin, C. M.; Voth, G. A. *Biochim. Biophys. Acta* **2010**, *1804*, 332−341.
(92) Sagnella, D. E.; Laasonen, K.; Klein, M. L. *Biophys. J.* **1996**, *71*, 1172−1178.
(93) Shepherd, L. M. S.; Morrison, C. A. *J. Phys. Chem. B* **2010**, *114*, 7047−7055.
(94) Cao, Z.; Peng, Y.; Yan, T.; Li, S.; Li, A.; Voth, G. A. *J. Am. Chem. Soc.* **2010**, *132*, 11395−11397.

(95) Moon, E. S.; Yoon, J.; Kang, H. *J. Chem. Phys.* **2010**, *133*, 044709.
(96) Churakov, A. V.; Prikhochenko, P. V.; Lev, O.; Medvedev, A. G.; Tripol'skaya, T. A.; Vener, M. V. *J. Chem. Phys.* **2010**, *133*, 164506.
(97) Feng, S.; Voth, G. A. *J. Phys. Chem. B* **2011**, *115*, 5903−5912.